Star-Shaped Wheel for Mechanical Micro-Doppler Modulation

Jordi Verdú, *Senior, IEEE,* Eloi Guerrero, *Student Member, IEEE,* Josep Parrón, Antonio Lázaro, *Senior, IEEE* and Pedro de Paco, *Senior, IEEE*

***Abstract*—This paper investigates the possibility of using star-shaped rotating wheels with deliberated geometries which provides unique micro-Doppler signature. Beyond the signature provided by the rotation rate of the target, additional information related with a particular target can be obtained taking advantage of specific and unique modulation waveforms. This feature can be very useful to increase detectability and classification and the approach can be used to generate warning signals in applications such automotive radars. Different star-shaped wheels with particular geometries have been designed demonstrating different reflection characteristics and modulation waveforms. The signature of these rotating star-shaped wheels has been measured in an anechoic chamber using a general purpose 24 GHz FMCW radar platform. As a detection method, an algorithm based on the derivative of the cross-correlation is proposed which validates the proposed approach.**

***Index Terms*—Frequency-Modulated Continuous Wave, Micro-Doppler, Radar**

I. Introduction

COMPARED with other radar configurations, Frequency-Modulated Continous Wave (FMCW) radars allow micro-dynamics (vibrations, rotations) identification due to their capability in micro-Doppler detection beyond range and relative velocity. The working principle of a FMCW radar is based on the transmission of a continuous frequency-modulated microwave signal that will be later mixed with the signal reflected from the target. Phase variations in consecutive chirp ramps provide precise information about a specific target reaching sub-λ resolution [1]. FMCW radars have been successfully used in human target detection and classification applications related to autonomous vehicle [2], [3], medical monitoring [4], [5], or retrieval of audio signals by measuring micro-vibrations [6] among others.

Micro-Doppler phenomena is related to a frequency modulation in the reflected signal when the target is under certain mechanical vibration or rotation. This feature has been very useful in order to classify or recognize the nature of different objects since the micro-Doppler signature can be related to specific geometric or dynamic characteristics [7]–[10]. The rotation-induced micro-Doppler modulation occurs when a certain target moves from a given position to a new one describing a rotation around a reference axis as it is the case of rotating blades [11], [12].

J. Verdú, E. Guerrero, J. Parrón and P. de Paco are with the Department of Telecommunications and Systems Engineering, Universitat Autònoma de Barcelona. 08193 Cerdanyola del Vallès, Spain: (Jordi.Verdu@uab.cat).

A. Lázaro is with the Electronics, Electrical and Automatics Engineering Department, Universitat Rovira i Virgili. 43007 Tarragona, Spain.

This work has been supported by the Spanish Secretaría de Estado de Investigación, Desarrollo e Innovación under Grant RTI2018-096019-B-C33.

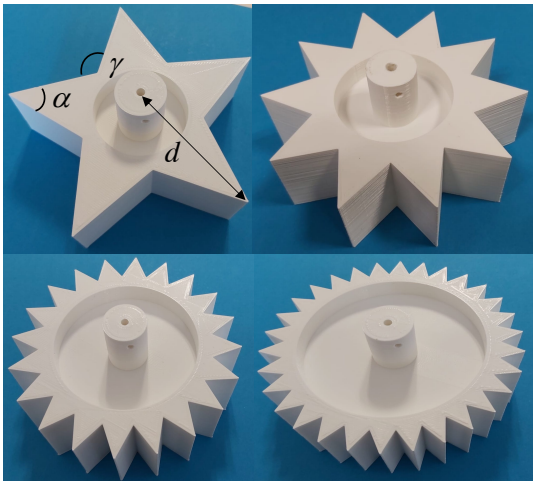

Fig. 1. 3D manufactured 5, 10, 20 and 30 tip star-shaped wheels prior to covering with copper layer.

Beyond the dynamic analysis of previous works, in this contribution we analyze, simulate and validate how the shape of the rotating target determines the time-dependent radar cross section (RCS) which takes the role of the modulation waveform. The spectrum of the IF signal is not only determined by the frequency allocation of side lobes, given by the rotation rate, but also by the amplitude which is directly related to the time-dependent RCS. This particular feature can be of interest in some applications, such as automotive radars, where unique micro-Doppler signatures can be generated to identify objects on the road and/or to avoid spoofing attacks.

In previous works [13], [14], it has been demonstrated that rotating elements can be used as warning signals (traffic control, road works signalling, etc...). In this work, instead of using 90 degrees rotating dihedral reflection corners, the influence of star-shaped geometries is investigated to obtain additional information from the target and thus improve the detectability. Taking advantage on the additive 3D manufacturing technologies, different star-shaped wheels in Fig. 1 have been designed with the objective to provide particular and specific modulation micro-Doppler signals by means of the particular time-dependent RCS. The wheels have been covered by an adhesive cooper layer to increase the reflectivity of the targets.

Since the modulation signal is mechanically generated, it is independent from operating frequency which may hinder electronic designs at high frequencies, for example in the 77

GHz band. Since the objective is to use these targets as a warning signals, the received IF signal will be known a priori, therefore, similarly to [15], a method based on the derivative of the cross-correlation between the reference (simulated) and the received (measured) has been implemented.

This contribution is organized as follows, the theoretical analysis of the received IF signal is carried out considering the time-dependence of the RCS is found in Section II. In Section III it is compared the previous simulation results with the measurements of rotating star-shaped wheels on an anechoic chamber with a 24 GHz FMCW radar. In Section IV an algorithm is proposed to carry out the signal detection based on the cross-correlation. Finally, the conclusions are presented in section V.

II. Mechanical Modulation by means of Time-dependent RCS

The basic mode of operation of the FMCW radar consists in the transmission of L chirps of duration T_c which will be later translated to intermediate frequency (IF). The chirp signal is defined by an amplitude A, the carrier frequency f_c and the chirp sweeping slope $\mu = B/T_c$, being B the bandwidth. The received signal will be delayed with an amplitude proportional to the radar cross-section σ of the target. For a simplified rotating target modelled using N backscatters, the IF signal can be obtained by the contribution of each one as [13],

$$x_{IF}(t) = A\sqrt{\sigma(t)}\prod\left(\frac{t}{T_c}\right)e^{-j2\pi\left(f_c\tau-\frac{\mu\tau^2}{2}\right)}e^{-j2\pi\mu\tau t} \quad (1)$$

In the case of the 90 degrees rotating dihedral reflection corners, the modulation waveform is very similar to an on-off keying (OOK) ASK modulation which is modelled by the term $e^{-j\beta\sin(\Omega_r t+\theta_0)}$ as developed in [13], where $\beta = 4\pi d/\lambda$ is the modulation index in FM signals (being d the radius of the wheel), and Ω_r is the rotation rate. However, our star-shaped wheel cannot be modelled in the same way because the walls reflect the incident electric field in a particular direction, or generate internal reflections between adjacent walls, triggering destructive or constructive interferences in the LOS of the radar. Therefore, the geometry of the target will have an influence on the modulation waveform. Due to the time-dependence of the RCS the theoretical approach in (1) is not precise enough to properly model the received IF signal.

To analyze the impact of the RCS on the received IF signal, four different star-shaped wheels with 5, 10, 20 and 30 tips, shown in Fig. 1, have been designed with radius d = 5.6 cm and tip angle α = 24° in all of them. With this geometric definition, the angle between adjacent walls γ is different in all the wheels and so is the corresponding RCS. The monostatic RCS has been obtained for each wheel by means of 3D simulation using FEKO software [16] as shown in Fig. 2. The incident angle at which maximum reflection occurs is different in all of them, as well as the monostatic RCS periodicity which is related to the number of tips N. Fig. 2 shows that all wheels generate strong echoes for that incident angles where one wall is perpendicular to the LOS of the radar.

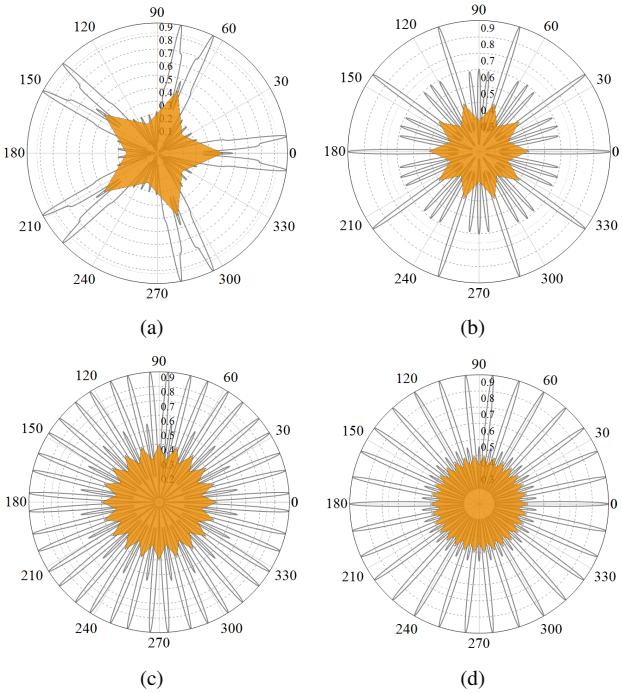

Fig. 2. Normalised polar representation of the monostatic RCS for the (a) 5 tip, (b) 10 tip, (c) 20 tip and (d) 30 tip star-shaped wheels respectively.

Taking into account the size of the target, d = 5.6 cm, as well as the operating frequency 24 GHz, far-field conditions can be assumed so the monostatic RCS in Fig. 3 is used to model the received IF signal. Otherwise, in a near-field scenario, the RCS should be computed as the integration of the electric field in the radiation pattern of the antenna. The resulting RCS has been normalized with respect its maximum value with the aim to compare the behaviour among the different wheels. The RCS is periodic for all the wheels. Depending on the angle between adjacent walls the number of RCS peaks can be N (N = 10 and 30) or $2N$ (N = 5 and 20). Of course, different geometries would lead different RCS behavior. This is an interesting feature to improve recognition.

Without loss of generality, the 20 tips star-shaped wheel has been simulated using different rotation rates Ω_r = 300, 800 and 1400 RPM. As shown in Fig. 4, and using the obtained RCS in Fig. 3 as modulation waveform, first side lobes are found at 100Hz, 266 Hz and 466 Hz respectively, being the consecutive second and third side lobes separated by $N\Omega_r$ which is in agreement with results in [17]. It is also important to highlight that the amplitude of side lobes does not depend on the Ω_r. The amplitude for first, second and third side lobes is coincident for all the rotation rates, and only depends on the modulation waveform. For $\Omega_r = 300$ RPM, the amplitude of the third side lobe is not perfectly aligned with the others as it occurs for higher rotation rates. This is due to the fact that this side lobe is approximately allocated in the limit of the modulation bandwidth which can be approximated as Bw $\approx 2(\beta+1)\Omega_r/2\pi$ [13]. For $\Omega_r = 300$ RPM (5 Hz), the third ($k = 3$) side lobe is allocated at $k\Omega_r N = 300$ Hz, being Bw ≈ 580 Hz (with $d = 5.7$ cm and f_0 = 24 GHz).

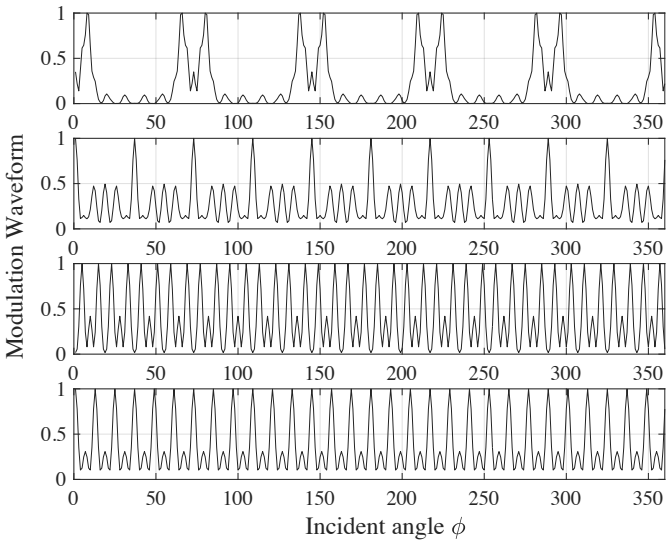

Fig. 3. Obtained RCS for the different wheels as a function of the incident angle ϕ. From top to bottom 5, 10, 20 and 30 tip star-shaped wheels.

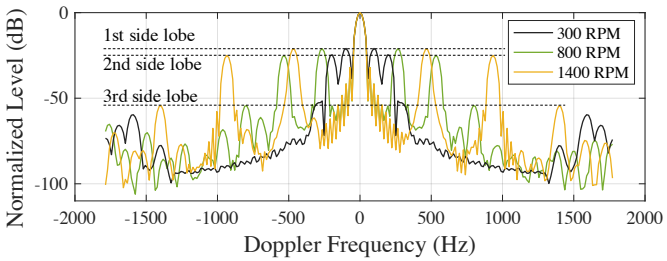

Fig. 4. Simulated received signal for 300 (solid black), 800 (dashed green) and 1400 (solid yellow) RPMs in the 20 tip star-shaped wheel.

From simulation results, it can be concluded that there is a trade-off between the rotation rate Ω_r, the radius d of the star-shaped wheel, and thus the modulation index β, for the detection or recognition of side lobes. For low Ω_r, it will be interesting to use star-shaped wheels with large number of tips N to increase separation between side lobes and facilitate the detection, and small N when the rotation rate is high. In case of using large N at high rotation rates, it will be necessary to use large values of d to increase the modulation bandwidth for detecting side lobes.

III. Measurements and Characterization of Star-shaped Wheels

For the experimental set-up, each wheel with $N = 5$, 10, 20 and 30 tips, has been mounted on a generic current-controlled DC motor in order to characterize different rotating rates in an anechoic chamber. The measurement set-up is shown in Fig. 5, where the distance between the radar and the rotating wheel is $R_0 = 2.6$ m. The measurements have been carried out using a general purpose 24 GHz FMCW DemoRad by Analog Devices and Inras. The operation bandwidth is 300 MHz leading to a velocity resolution of Δv = 0.162 m/s, equivalently Δf_D = 12.9 Hz for a $T_c = 280$ μs.

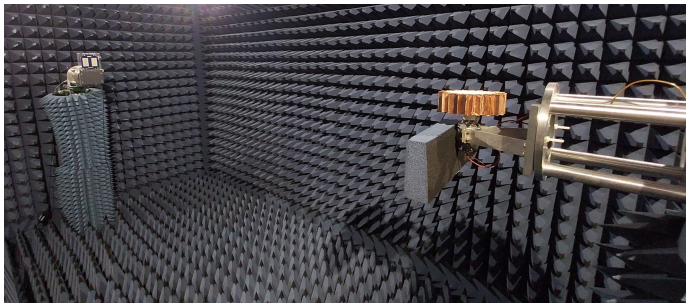

Fig. 5. Characterization set-up inside the anechoic chamber. The distance between the radar and the rotating wheel is $R_0 = 2.6$ m.

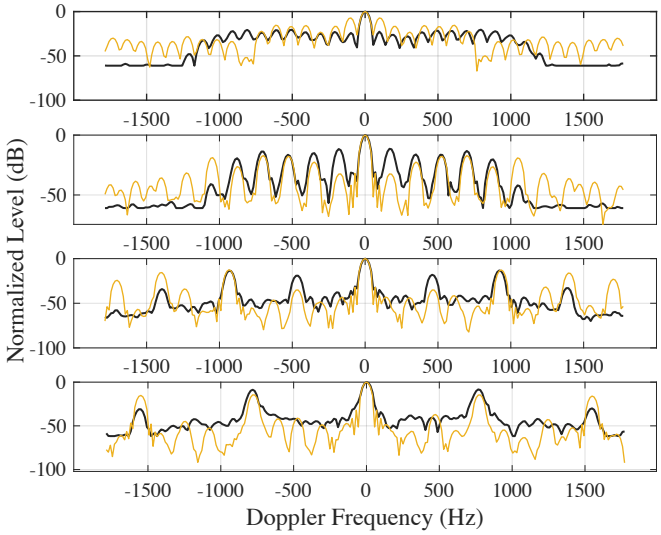

Fig. 6. Comparison between measurement (black) and simulation (yellow) received signal for the 5 (@1000RPM), 10 (@1100RPM), 20 (@1400RPM) and 30 (@1550RPM) tip star-shaped wheels (from top to bottom).

The 5, 10, 20 and 30 tip star-shaped wheels have been measured at Ω_r = 1000, 1100, 1400 and 1550 RPMs respectively. As shown in Fig. 6, there is a good agreement with theoretical simulations. The allocation of the frequency lobes, given by the product $N\Omega_r$, agrees with the theoretical prediction. The discrepancy in the amplitude of some lobes may come from vibrations in the elevation plane due to some vibration in the plane of rotation non considered in the theoretical model. For sake of clarity in the comparison, the received signal level has been normalized in all cases.

IV. Method for Detection of Rotating Star-shaped Wheels

The good agreement between simulation and measurement, particularly in the allocation of the frequency lobes as well as the modulation bandwidth, allows to propose a detection method based on the derivative by finite differences of the cross-correlation $R_{zx}[n]$ in the discrete frequency domain between the reference (simulation) $X[n]$ and the received (measurement) signal $Z[n]$ as,

$$R_{xz}[n] = X[n] \star Z[n] \triangleq \sum_{m=-\infty}^{\infty} X^*[m]Z[m+n] \quad (2)$$

being * the conjugate operator.

Different experiments have been carried out in order to validate the proposed detection method. First, a reference signal corresponding to a 20-tip star-shaped wheel has been compared with the measurements for wheels with $N = 10$ (green), N =20 (yellow) and N =30 (purple) tips in Fig. 7(a). Since the wheels are different (different N), for the same Ω_r the lobes are not coincident. Therefore, different Ω_r has been set in each wheel (1250, 1380 and 1810 RPM respectively) in such a way some lobes are coincident with the lobes in the reference signal which increases the complexity in the detection of the target. The result of the cross-correlation R_{xz} shows that the highest value along the samples corresponds to the one related with the $N = 20$ tips wheel as expected. Moreover, the most interesting issue is the presence of peaks separated a distance of $N\Omega_r$, that is, at those positions where all the lobes are coincident. This only happens for the case where the number of tips as well as the rotation rate is coincident. Therefore, the derivative of the cross-correlation R'_{xz} can be used to determine the most-likely signal by the inspection of the peaks with the highest level as shown in the bottom of Fig. 7(a).

A second experiment has been carried out using the wheel with 20 tips with different rotation rates. The signal to be detected is the one provided by a wheel at 1380 RPM (yellow trace). A reference signal with 1400 RPM has been used (grey dot-dash line) which is slightly different from the signal to be detected to emulate some drift in the Ω_r value.

The cross-correlation R_{xz} shows the presence of different peaks as before. However, the measurements of wheels at 1100 and 800 RPM (green and blue respectively) result in a higher level of cross-correlation which may be not suitable to carry out a successful detection. However, as previously commented, the derivative provides unambiguous detection because the peaks only appear when the distance between lobes $N\Omega_r$ is coincident. This is shown in the bottom of Fig. 7(b) where the peaks with the highest level corresponds to the yellow trace, the one with the RPMs closer to the reference. Then, the peak detection can be easily associated to the expected signal to be received.

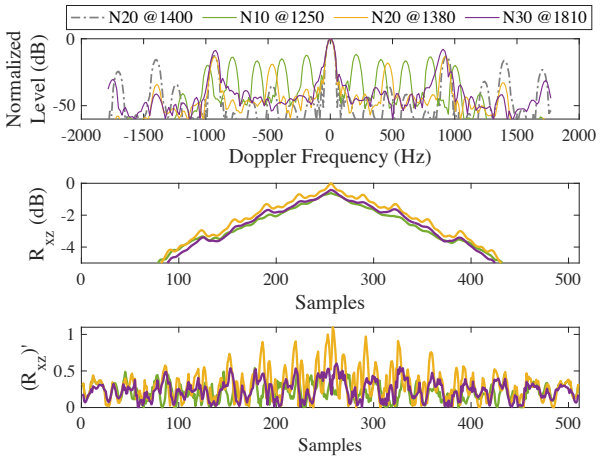

(a)

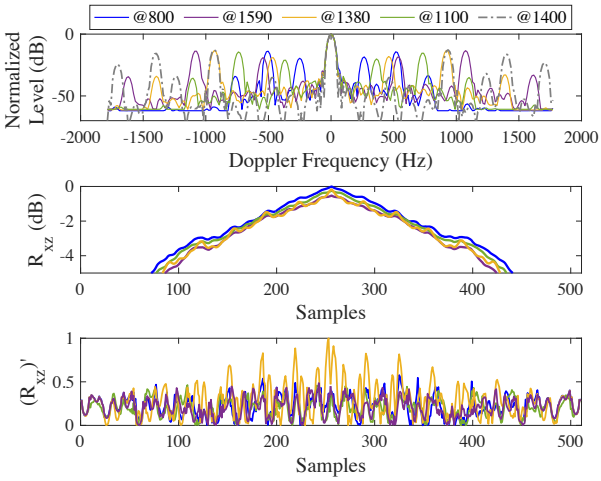

(b)

Fig. 7. (Top) Comparison between the reference signal (grey dot-dash line) and measured received signals, (middle) Cross-correlation between the reference signal and measurements, (bottom) derivative of the cross-correlation. (a) Results for star-shaped wheels with different number of tips N, (b) Results for a 20 tip wheel at different rotation rates.

V. Conclusion

In this paper, it has been demonstrated that specific geometric shapes may lead to a particular modulation waveform in rotating targets. To this aim, star-shaped wheels with different number of tips have been designed and tested. The allocation of the frequency side lobes in the IF signal is directly related to the rotation rate, being the separation determined by the product between the number of tips and the rotation rate. However, depending on the modulation waveform, given by a certain geometry, the amplitude of side lobes may be different and not dependent on the rotation rate. This particular behaviour may improve classification and identification of rotating targets. Simulation results have been validated by means of experimental characterization of different star-shaped wheels using a general purpose 24 GHz radar platform. A detection method based on the derivative of the cross-correlation of a reference signal and the signal to be detected has been proposed. The method has been successfully applied to scenarios where a reference signal is compared with the expected measured signal and other signals provided by star-shaped wheels with different rotation rates or different number of tips. In all cases the signal with the highest cross-correlation is the expected one which demonstrates the reliability of the proposed approach.

Acknowledgment

The authors would like to thank the OpenLabs at Universitat Autònoma de Barcelona for the support in the manufacturing of the star-shaped wheels allowing the use of the additive manufacturing tools and techniques.

References

[1] M. Skolnik, *Introduction to radar systems*. Boston: McGraw Hill, 2001.

[2] E. Hyun, Y.-S. Jin, and J.-H. Lee, "Moving and stationary target detection scheme using coherent integration and subtraction for automotive FMCW radar systems," in *2017 IEEE Radar Conference (RadarConf)*. IEEE, may 2017.

[3] C. Will, P. Vaishnav, A. Chakraborty, and A. Santra, "Human target detection, tracking, and classification using 24-GHz FMCW radar," *IEEE Sensors Journal*, vol. 19, no. 17, pp. 7283–7299, sep 2019.

[4] M. Alizadeh, G. Shaker, J. C. M. D. Almeida, P. P. Morita, and S. Safavi-Naeini, "Remote monitoring of human vital signs using mm-wave FMCW radar," *IEEE Access*, vol. 7, pp. 54 958–54 968, 2019.

[5] H. Lee, B.-H. Kim, J.-K. Park, S. W. Kim, and J.-G. Yook, "A resolution enhancement technique for remote monitoring of the vital signs of multiple subjects using a 24 ghz bandwidth-limited FMCW radar," *IEEE Access*, vol. 8, pp. 1240–1248, 2020.

[6] E. Guerrero, J. Brugues, J. Verdu, and P. de Paco, "Microwave microphone using a general purpose 24-GHz FMCW radar," *IEEE Sensors Letters*, vol. 4, no. 6, pp. 1–4, jun 2020.

[7] V. Chen, F. Li, S.-S. Ho, and H. Wechsler, "Micro-doppler effect in radar: phenomenon, model, and simulation study," *IEEE Transactions on Aerospace and Electronic Systems*, vol. 42, no. 1, pp. 2–21, jan 2006.

[8] S. Ram and H. Ling, "Microdoppler signature simulation of computer animated human and animal motions," in *2008 IEEE Antennas and Propagation Society International Symposium*. IEEE, jul 2008.

[9] R. Mamgain, R. Jain, and D. Deb, "Study and simulation of radar targets micro-doppler signature," in *2018 International Conference on Radar (RADAR)*. IEEE, aug 2018.

[10] J. Gong, J. Yan, D. Li, R. Chen, F. Tian, and Z. Yan, "Theoretical and experimental analysis of radar micro-doppler signature modulated by rotating blades of drones," *IEEE Antennas and Wireless Propagation Letters*, vol. 19, no. 10, pp. 1659–1663, oct 2020.

[11] Z. Zhou and J. Huang, "X-band radar cross-section of tandem helicopter based on dynamic analysis approach," *Sensors*, vol. 21, no. 1, p. 271, jan 2021.

[12] T. Peto, S. Bilicz, L. Szucs, S. Gyimothy, and J. Pavo, "The radar cross section of small propellers on unmanned aerial vehicles," in *2016 10th European Conference on Antennas and Propagation (EuCAP)*. IEEE, apr 2016.

[13] A. Lazaro, M. Lazaro, R. Villarino, and P. D. Paco, "New radar micro-doppler tag for road safety based on the signature of rotating backscatters," *IEEE Sensors Journal*, vol. 21, no. 6, pp. 8604–8612, mar 2021.

[14] A. Lazaro, M. Lazaro, R. Villarino, D. Girbau, and P. de Paco, "Car2car communication using a modulated backscatter and automotive FMCW radar," *Sensors*, vol. 21, no. 11, p. 3656, may 2021.

[15] W. Y. Yang, J. H. Park, J. W. Bae, N. H. Myung, and C. H. Kim, "Automatic algorithm for estimating the jet engine blade number from the radar target signature of aircraft targets," *IEEE Aerospace and Electronic Systems Magazine*, vol. 30, no. 7, pp. 18–29, jul 2015.

[16] *www.altair.com/feko*.

[17] V. Chen, "Analysis of radar micro-doppler with time-frequency transform," in *Proceedings of the Tenth IEEE Workshop on Statistical Signal and Array Processing (Cat. No.00TH8496)*. IEEE, 2020.